Turkish Journal of Electrical Engineering & Computer Sciences

http://journals.tubitak.gov.tr/elektrik/

Research Article

Turk J Elec Eng & Comp Sci
(2015) 23: 1449 – 1464

doi:10.3906/elk-1306-193

Optimal IPFC damping controller design based on simplex method and self-tuned fuzzy damping scheme in a two-area multimachine power system

Ahmet Mete VURAL[1,*], **Kamil Çağatay BAYINDIR**[2]

[1]Department of Electrical and Electronics Engineering, Faculty of Engineering, University of Gaziantep, Gaziantep, Turkey

[2]Department of Energy Systems Engineering, Faculty of Engineering, Yıldırım Beyazıt University, Adana, Turkey

Received: 21.06.2013 • **Accepted/Published Online:** 17.09.2013 • **Printed:** 28.08.2015

Abstract: This paper develops a novel self-tuned fuzzy damping control scheme for an interline power flow controller (IPFC) to suppress the interarea mode of oscillations in a multimachine power system. The nonlinear adaptive damping controller is based on coordinated operation of two fuzzy inference systems. The first one produces the required q-axis voltage reference of the quasi multipulse series converter in response to generator angle oscillations, while the second one is used to tune the output of the first one online for further reducing the error signal using a given set of fuzzy rules. The simplex method is employed to search for optimal gains of the damping controller by minimizing the objective function in which speed deviations between generators are formulated. The feasibility of the proposed technique is validated using time-domain simulation cases in the PSCAD simulation program. It is also shown that the proposed damping scheme for IPFC works better than the static synchronous series compensator, which utilizes the same damping scheme in reducing the interarea mode of oscillations.

Key words: Interline power flow controller, static synchronous series compensator, quasi multipulse converter, self-tuned fuzzy damping control, simplex method, transient stability, interarea mode of oscillation

1. Introduction

The interarea mode of oscillations occurs at 0.1–0.8 Hz when the power system is subjected to faults due to the dynamic interactions of synchronous machines that are widely geographically separated [1–3]. The problem worsens when power networks are more interconnected and the level of power transfer is increased through weak transmission corridors. These oscillations may be sustained and may grow, which leads to partial or total power interruption if no adequate damping is provided. Although conventional power system stabilizers (PSSs) are widely used by power system utilities, their use cannot develop sufficient damping to interarea modes and more efficient alternatives are needed other than PSSs [4]. In this study, two members of the converter-based FACTS devices are considered for oscillation damping: the interline power flow controller (IPFC) [5–8] and static synchronous series compensator (SSSC) [9–11].

In general, IPFC studies are mostly based on an average model that is the approximated approach of the converter dynamics in which the discrete-time nature of the converter switching and the effects of harmonics are neglected. DC link dynamics are modeled as a power balance equation in terms of dq components of voltage

*Correspondence: mete.vural@gaziantep.edu.tr

and current. The IPFC average models are used in single-machine infinite-bus systems [12–17] or multimachine systems [18–20].

According to literature review results, applying IPFC average models to stability studies is well known and broad, but IPFC converter-level models are limited. The key work presented in this study covers the use of a converter-level modeling approach by designing high-power quasi multipulse converters for IPFC in a time-domain simulation platform and the design of a novel self-tuned model-free damping control scheme for the IPFC to mitigate the interarea mode of oscillations in a multimachine power system.

2. IPFC configuration

An IPFC can concurrently control real power flows of two parallel lines (P_{Line1}, P_{Line2}) and a selected reactive power flow (Q_{Line1} or Q_{Line2}), as shown in Figure 1. DC link voltage (E) is controlled by VSC1. Each VSC synthesizes AC voltage having controllable magnitude (V_{se1}, V_{se2}) and controllable phase shift (θ_{se1}, θ_{se2}). P_{inj1} and P_{inj2} are the real power injections of VSC1 and VSC2, respectively. Similarly, Q_{inj1} and Q_{inj2} are the reactive power injections of VSC1 and VSC2, respectively. The DC link, represented by capacitor C, enables real power exchange ($P_{t1\&2}$) among converters. P_{loss1} and P_{loss2} are the sum of switching losses and coupling transformer losses of VSC1 and VSC2, respectively.

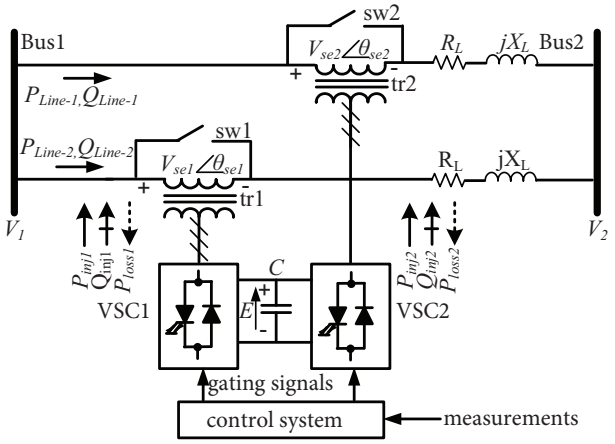

Figure 1. IPFC configuration.

3. Quasi multipulse converter design

3.1. Power circuit

Figure 2 shows the quasi multipulse converter to be operated as each VSC of the IPFC [21]. The quasi multipulse topology consists of eight two-level six-pulse VSCs fed from a DC link and three types of magnetic interfaces. To keep converter switching as low as possible (i.e. line frequency switching), two converter groups, Group-A and Group-B, are considered, each of which consists of four six-pulse converters, 1–4 and 5–8, respectively. The function of magnetic interface-1 is to obtain a three-phase twelve-pulse voltage waveform by connecting the AC outputs of the two neighboring converters. Phase shift angle between two adjacent twelve-pulse converters should be 7.5°, so 7.5°, 0.0°, –7.5°, and –15° phase shifts are applied to the gating signals of each upper six-pulse converter of twelve-pulse units 1, 3, 2, and 4, respectively. Gating signals of each lower six-pulse converter of four twelve-pulse units are shifted by 30° one by one with respect to each upper-side VSC for twelve-pulse operation. Group-A involves two separate twelve-pulse configurations, which are combined by two

magnetic interfaces-1 to obtain quasi 24-pulse voltage waveform. The same situation also applies to Group-B. Magnetic interface-2 sums up each phase of Group-A with that of Group-B. Magnetic interface-3 is used to add one phase of the quasi 24-pulse waveform of Group-A with the same phase of the quasi 24-pulse waveform of Group-B. Magnetic interface-3 inserts each phase of the quasi multipulse voltage waveform into the respective phase of the transmission line in series.

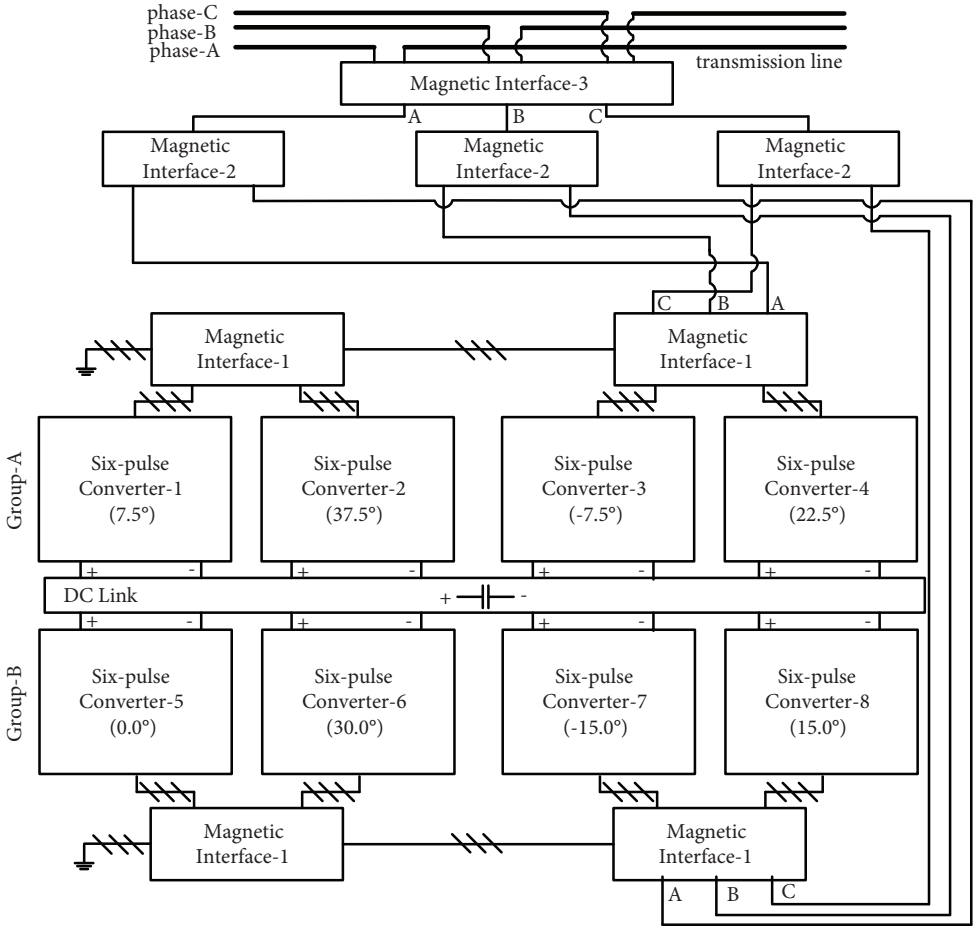

Figure 2. Schematic diagram of the series quasi multipulse converter topology.

3.2. Control scheme

The voltage of the line frequency switched quasi multipulse converter can be fully controllable both in magnitude and phase angle only if the three-phase voltage waveforms of Group-A and those of Group-B become controlled out of phase as illustrated in Figure 3a. The desired voltage vector of the quasi multipulse converter V_X can then be obtained by summing the output voltage vectors of Group-A and Group-B (V_A, V_B). The desired phase angle of Group-A ($\alpha - \delta$ with respect to the d-axis) and that of Group-B ($\alpha + \delta$ with respect to the d-axis) are formulated by the following equations [22]:

$$\alpha = \tan^{-1} \sqrt{\frac{(2V_F)^2 - \left(V_D^{ref}\right)^2 - \left(V_Q^{ref}\right)^2}{\left(V_D^{ref}\right)^2 + \left(V_Q^{ref}\right)^2}}, \tag{1}$$

$$\delta = \tan^{-1} \frac{V_Q^{ref}}{V_D^{ref}}. \tag{2}$$

Since the magnitudes of V_A and V_B are constant (Group-A and Group-B are fed from a constant DC link voltage), the desired magnitude and phase angle of V_X can only be obtained by controlling α and δ in real time. In Eqs. (1) and (2), V_F can be considered as the average converter voltage (V_F $=0.5(V_A + V_B)$) to minimize measurement variations [21]. V_D^{ref} and V_Q^{ref} are the desired direct and quadrature axis components of voltage vector V_X, respectively. The desired axis components are computed using IPFC control loops.

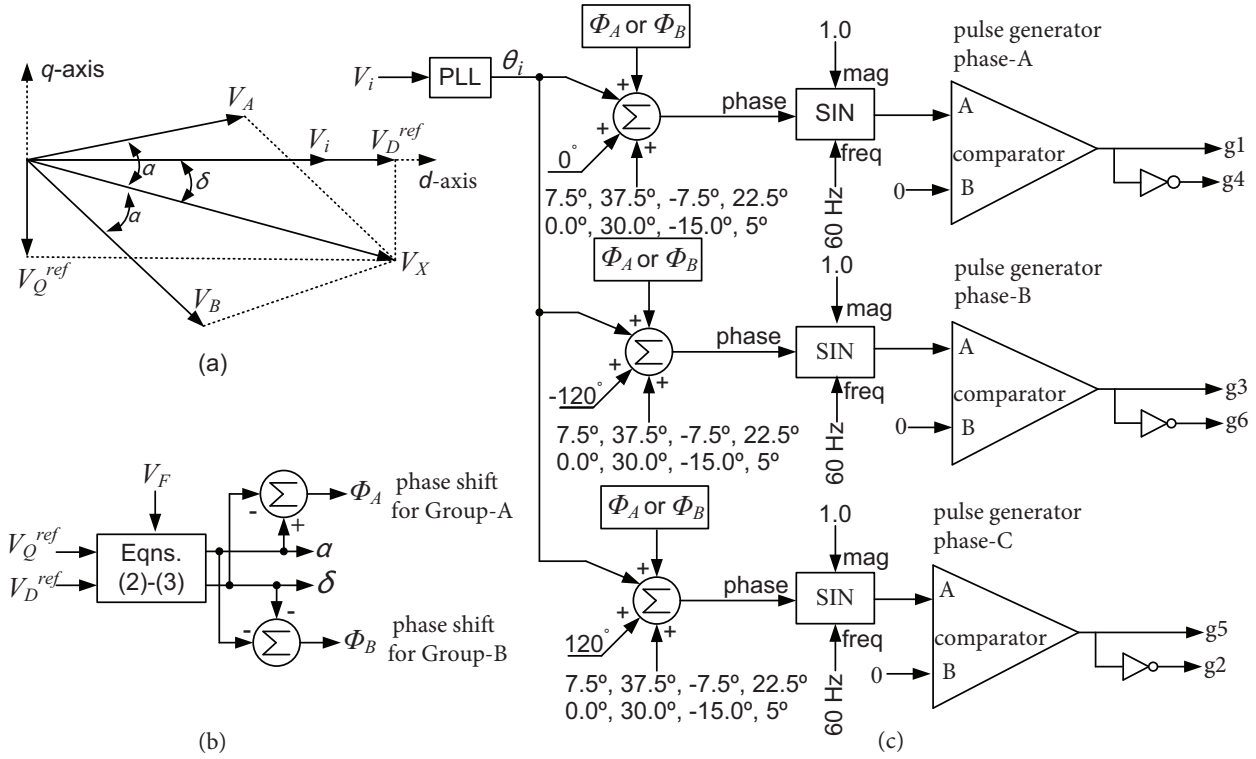

Figure 3. (a) Voltage vectors of Group-A and Group-B in synchronous rotating frame, (b) phase shift calculation, (c) six-pulse circuit.

3.3. Pulse generation

The pulse circuit shown in Figures 3b and 3c generates square waveforms for GTO-thyristor switching in a six-pulse converter and 60 Hz sinusoidal signal with amplitude one is compared with zero. Hence, for the first half-cycle of fundamental frequency the comparator output becomes logical high, and for the second half-cycle the comparator output becomes logical low. The produced square-wave is phase shift controlled since the phase shift of the sinusoidal signal can be externally controlled by the signal phase depending on the position of the six-pulse converter unit in quasi multipulse topology. Hence, the total number of required pulse circuits is sixteen for IPFC operation.

4. Self-tuning fuzzy damping controller

Figure 4 shows the self-tuning fuzzy damping controller (STFDC) structure, which is based on a self-tuning fuzzy-PI control scheme [23,24]. The STFDC consists of two concurrently operating fuzzy modules, i.e. a fuzzy damping controller (FDC) and fuzzified gain tuner (FGT). A PSCAD module written in Fortran is used to link PSCAD with MATLAB so that both programs can exchange information online at every solution time step of PSCAD. Membership functions and fuzzy rules of the STFDC are shown in Figure 5. In the FDC, error signal e and its derivative Δe at sample k are formulated in Eqs. (3) and (4), respectively. K_{w1} and K_{w2} are the damping gains; w_1, w_2, and w_3 are the generator speeds at sample k, which are geographically aligned in three different locations.

$$e(k) = P_{line}^{ref} - P_{line} + K_{w1}(w_2 - w_1) + K_{w2}(w_3 - w_1) \tag{3}$$

$$\Delta e(k) = e(k) - e(k-1) \tag{4}$$

In Eqs. (3) and (4), e and Δe are respectively multiplied by simplex optimized gains (a_1, a_2) to be mapped to their equivalent fuzzy values by the membership functions of the knowledge base of the FDC.

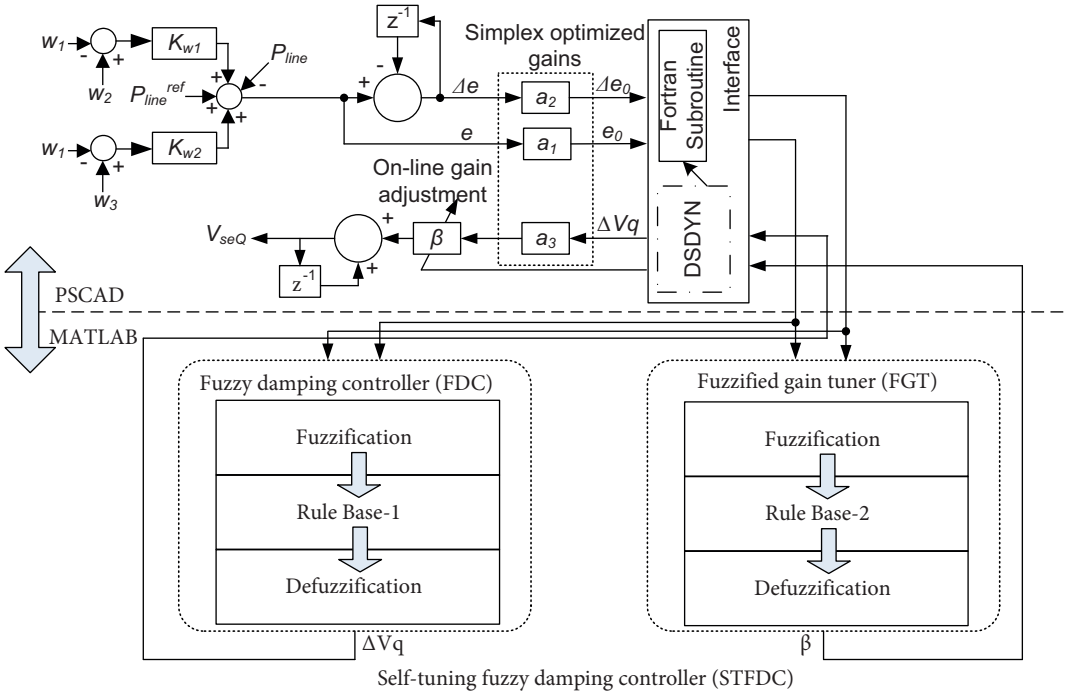

Figure 4. Schematic diagram of STFDC.

Membership functions are symmetrical triangles (except the two at both ends) that have equal 50% base overlap and divide the domain [–1, 1] into seven equal regions. The cell defined by the intersection of the first row and the first column represents a rule such as {"If Δe_0 is P1 and e_0 is N2 then ΔV_q is N1"}. The antecedents are evaluated by applying the "*min*" operator and the output fuzzy set is truncated by applying the "*min*" implication operator. The fuzzy sets are aggregated into a single fuzzy set by the "*max*" operator that should be later defuzzified to resolve a single real-number signal for ΔV_q. Centroid defuzzification method is applied to get incremental change in the q-axis component of the series VSC. The formulation is given in Eq. (5):

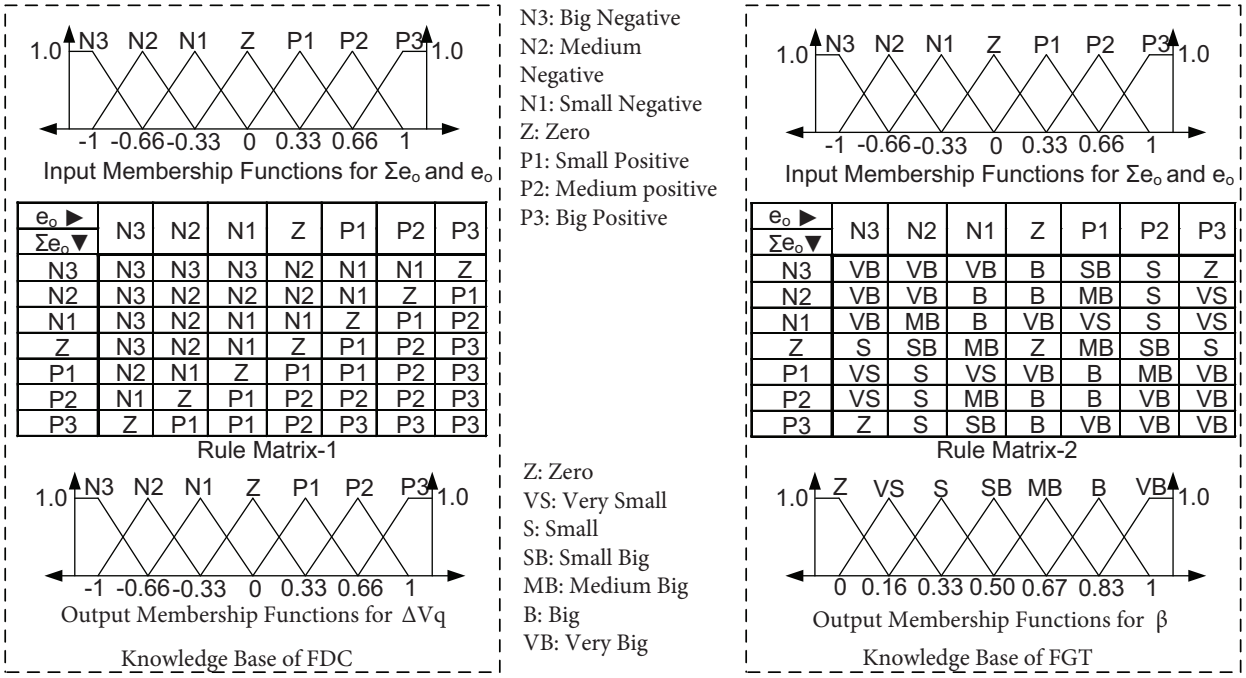

Figure 5. Membership functions and fuzzy rules for STFDC.

$$\Delta V_q(k) = \frac{\sum_{i=1}^{49} b_i \int \mu(i)}{\sum_{i=1}^{49} \int \mu(i)}, \tag{5}$$

where $\mu(i)$ and b_i are the output membership function and the center of the output membership function of the consequent of rule i, respectively. At sample k, V_q is calculated in Eq. (6) where $\beta$is the online gain factor determined by FGT.

$$V_q(k) = V_q(k-1) + a_3 \beta \Delta V q(k) \tag{6}$$

The value of β is computed by a nonlinear mapping function described by the rule matrix-2 of the FGT whose structure is the same for its fuzzy operators and input membership functions as that of the FDC. The universe of discourse for β lies in the domain [0, 1] and is obtained by shifting and scaling (add 1 and multiply by 0.5) input membership functions of the FDC along the horizontal axis. Rule matrix-2 is designed to improve the damping performance of the IPFC under large disturbances such as a three-phase fault on the transmission network. For instance, after a fault occurs, the error may be small-positive (P1) but he error-integral can be sufficiently large (P3). In this case, β should be big enough (VB) to increase converter voltage. Under such a situation, the rule is {"If Δe_0 is P3 and e_0 is P1 then β is VB"} . The control surfaces of the proposed STFDC are shown in Figure 6.

4.1. Tuning of scaling factors

The scaling factors (a_1, a_2, a_3) are used to normalize input and output variables of the FDC. Commonly, there is no well-defined method for selection of scaling factors [23]. In this study, these parameters are optimized by simplex optimization method. The cost function is based on the integral time absolute errors of the generator speeds given in Eq. (7). t is the current simulation time, t_0 is the fault time, and T is the total simulation time

of the given case study (Case 1). In the case of the IPFC, the value of f is minimized from 0.2078 to 0.0399 in 97 iterations for a tolerance of 1.0E-6. In the case of the SSSC, the value of f is minimized from 0.2452 to 0.2221 in 60 iterations for the same tolerance value. The convergence performance of the simplex method when only the FDC is executed while the FGT is deactivated is shown in Figure 7 for both FACTS devices. The optimized parameters are listed in Table 1.

$$f(a_1, a_2, a_3) = \int_{t=t_0}^{T} (t \cdot |w_1 - w_2| + t \cdot |w_1 - w_3|) \cdot dt \tag{7}$$

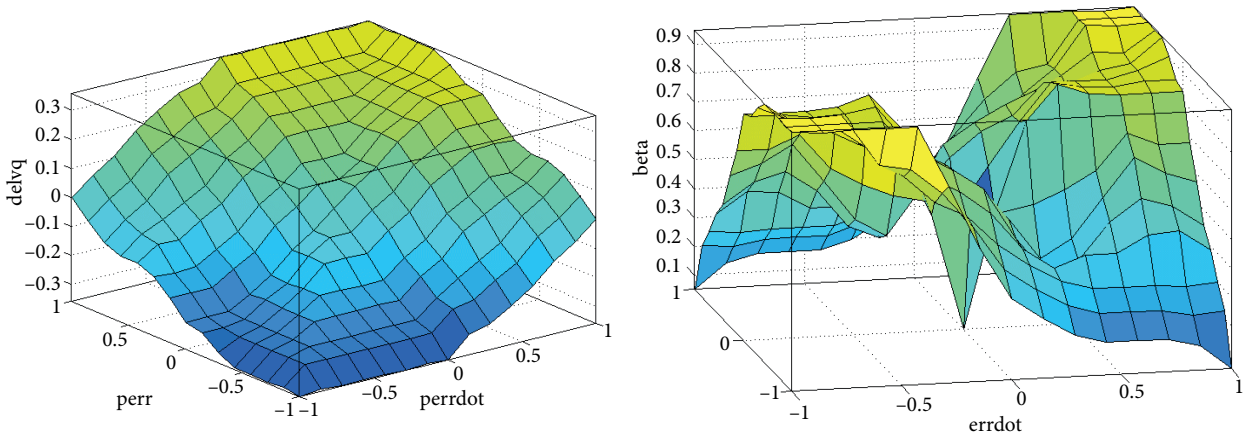

(a) FDC (b) FGT

Figure 6. Control surfaces of the proposed STFDC.

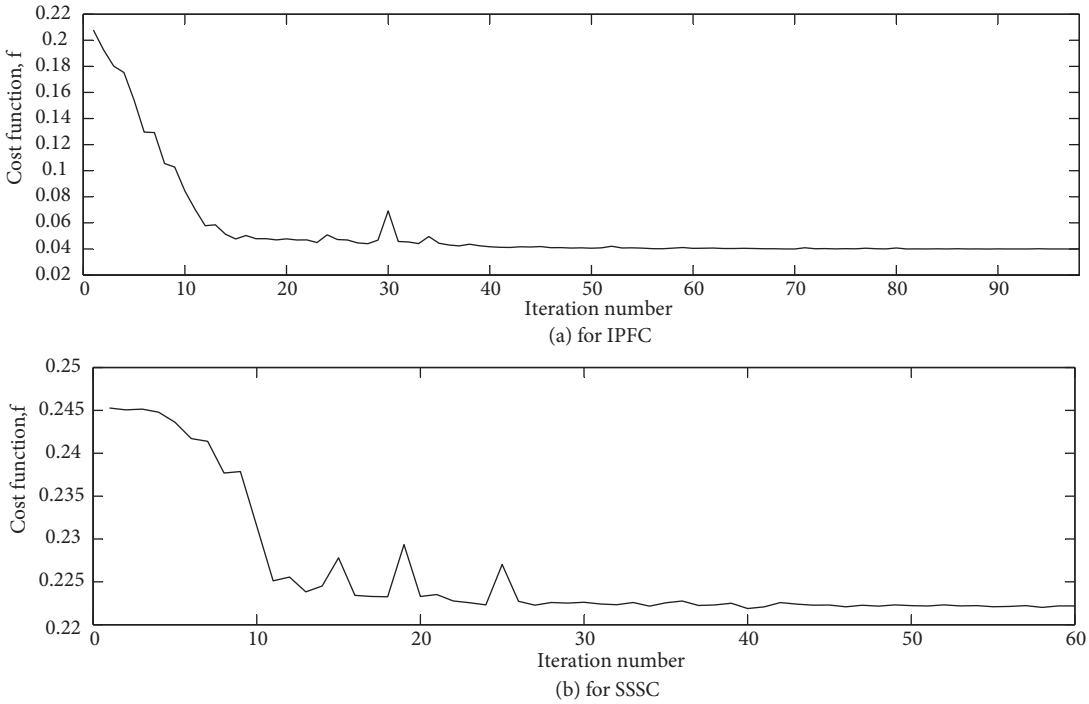

(a) for IPFC

(b) for SSSC

Figure 7. Convergence performance of the simplex method.

Table 1. Optimized scaling factors.

Scaling factors	IPFC	a_1	a_2	a_3	SSSC	a_1	a_2	a_3
Initial guess		0.1	0.1	0.1		0.1	0.1	0.1
Converged result		0.6	0.6	3.67		0.75	0.45	4.60

5. Simulation results

The two-area power system embedded with the IPFC and its control scheme are modeled in PSCAD and shown in Figure 8. The two generation areas are represented by aggregate machines, which are connected together via a double transmission line intertie. IPFC is activated for Lines 1 and 2 when switches sw1 and sw3 are opened and sw2 is closed. SSSC is activated on Line 2 when switches sw2 and sw3 are opened and sw1 is closed. Ten, 5, and 8 aggregated synchronous generators (SGs), rated 120 MVA each, are operated in parallel to produce 1200 MVA (G1), 600 MVA (G2), and 960 MVA (G3) output, respectively. Each SG is driven by a hydrogovernor with a solid-state exciter. Transmission line data are given as follows: $R = 0.178159$E-4 Ω/m, $X = 0.31388$E-3 Ω/m, and $B = 273.5448$ MΩ/m. The solution time step of PSCAD is set to 100 μs.

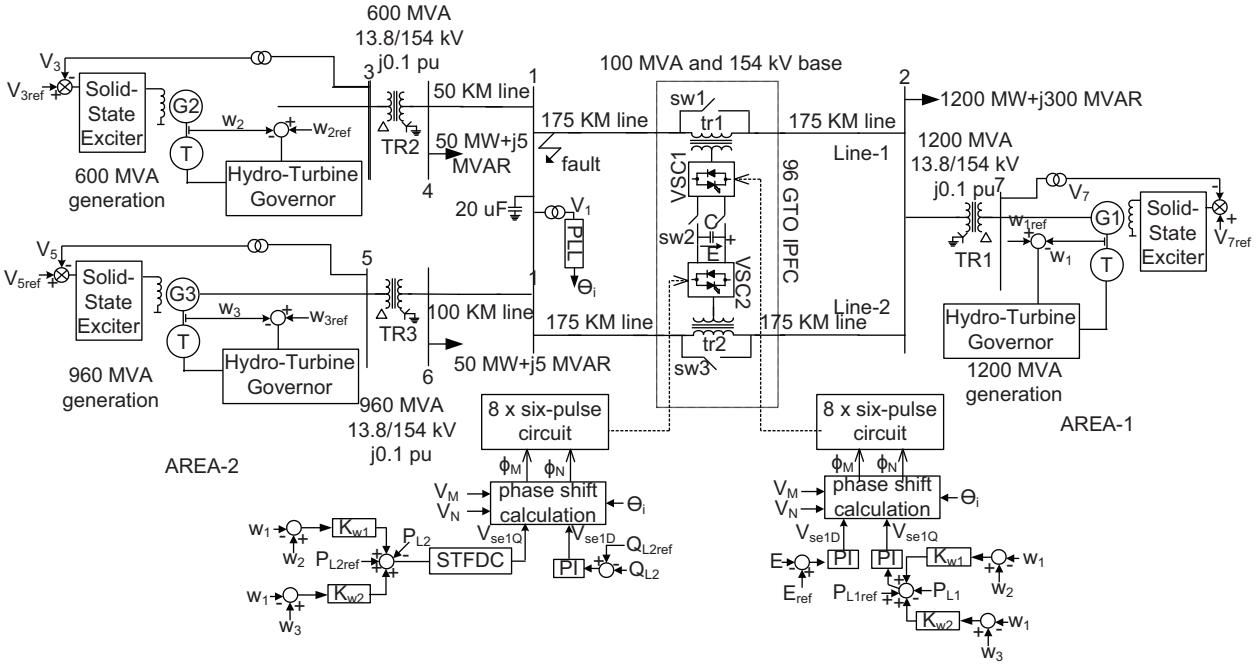

Figure 8. Two-area system embedded with IPFC and IPFC control scheme.

The system stability is investigated without any FACTS device, with the IPFC, and with the SSSC by applying different types of line faults with different durations. The impact of faults is also investigated on the performances of the control loops of the IPFC and SSSC. PI controller parameters (proportional gain, integral time constant) are 1.0, 0.001 for the real power flow controller of the VSC1; 0.2, 0.001 for the real power flow controller of the VSC2; 0.1, 0.001 for the DC voltage controller; and damping gains $K_{w1} = K_{w2} = 500$; $C = 0.2$ F. Steady-state uncontrolled real power flows of the intertie are 0.975 pu for each transmission line. The performance of the STFDC for both the IPFC and SSSC is examined individually for the same disturbance conditions applied to the two-area system, which leads to interarea mode of oscillations in conjunction with the following dynamic control tasks of the IPFC or SSSC:

- Line 1 real power flow by VSC1 of IPFC,
- Line 2 real power flow by VSC2 of IPFC,
- DC link voltage by VSC2 of IPFC,
- Line 2 real power flow by VSC2 of IPFC (or SSSC),
- DC link voltage by VSC2 of IPFC (or SSSC).

5.1. Case 1: Three-phase to ground fault

Before disturbance, the reference values of tie-line flows *PLine-1* and *PLine-2* are respectively set to 1.1 pu and 1.2 pu at the real power flow controllers of the IPFC while the DC link voltage is regulated at 1.4 kV. The same reference value of *PLine-2* is set for the SSSC's real power flow controller and then a three-phase to ground fault near Bus 1 on *Line-1* with 140 ms of duration is applied at $t = 2.0$ s. As shown in Figures 9a and 9b, the angle oscillations of generators G2 and G3 with respect to generator G1 are cumulative and lead to unstable operation when no FACTS device is activated. The SSSC, having only VSC2, exhibits weakly damped interarea modes at approximately 0.50 Hz for both G2 and G3 with respect to G1. On the other hand, the IPFC, having both VSC1 and VSC2, effectively damps out the oscillations caused by this severe disturbance in a relatively short duration. Comparing the responses of the IPFC to the SSSC compensation scheme in Figures 9c and 9d, the positive contribution of the proposed STFDC adapted for the IPFC is clear when controlling intertie real power flows caused by interarea oscillations. Figure 9e shows that the time responses of the DC link voltage of both the SSSC and IPFC are practically the same, which is highly required for proper VSC operation. Figure 9f shows reactive power flow fluctuations on *Line-1* caused by three-phase disturbance when reactive power flow control function of the IPFC is disabled to make a fair comparison to the SSSC. Figures 9g and 9h show that the STFDC-equipped IPFC better improves bus voltage profiles of the intertie with smoother responses following three-phase fault when compared with the STFDC-equipped SSSC. Figures 10 and 11 show some selected time domain signals of the two VSCs of the IPFC, which reveal stable converter operation.

5.2. Case 2: Two-phase to ground fault

The system is disturbed by a two-phase (phases B and C) to ground fault near Bus 1 on *Line-1* for 160 ms duration at $t = 2.0$ s, while keeping the same predisturbance steady-state operating conditions as in Case 1. The system is unstable when there is no compensation applied. Figures 12a and 12b show the responses of generators G2 and G3 with respect to generator G1 when the SSSC with STFDC is applied and when the IPFC with STFDC is applied. The comparative time-domain results show that the stabilizing function of the IPFC for interarea oscillations is superior to that of the SSSC even when the STFDC is adapted individually to both FACTS devices by optimizing its scaling factors. The IPFC with STFDC easily stops the real power oscillations both on *Line-1* and *Line-2* and forces them to their steady-state controlled values as shown in Figures 12c and 12d. When a particular comparison between Figure 9c and Figure 12c is made, the SSSC weakly suppresses power oscillation in the case of two-phase to ground fault due to the longer duration of the fault. The DC link voltage controllers of both the SSSC and IPFC give practically the same response to the short circuit as shown in Figure 12e. Figure 12f shows reactive power flow fluctuations on *Line-1* when the IPFC and SSSC are operated separately when the reactive power flow control function of the IPFC is disabled. Accordingly, as in Case 1, the fluctuations are less as in the case of the IPFC when compared with the SSSC. Figures 12g and 12h

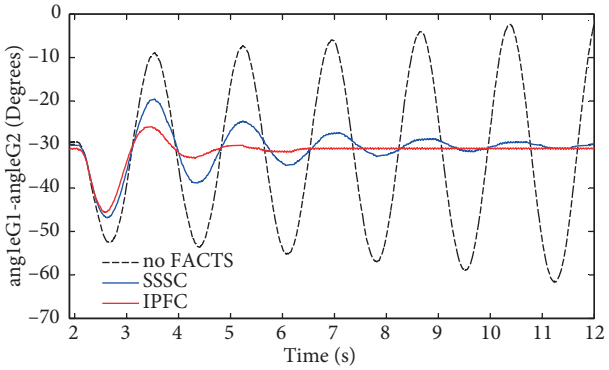

(a) Transient response of generator G2 rotor angle, measured with respect to generator G1 rotor angle following three-phase fault

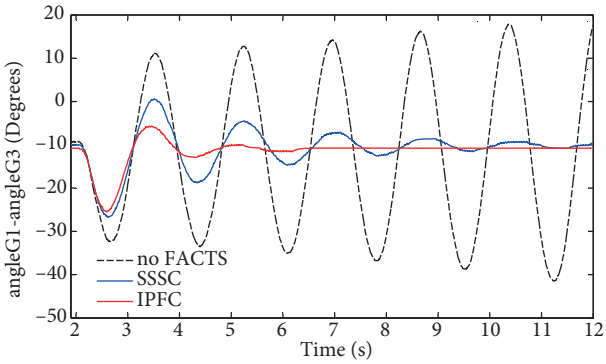

(b) Transient response of generator G3 rotor angle, measured with respect to generator G1 rotor angle following three-phase fault

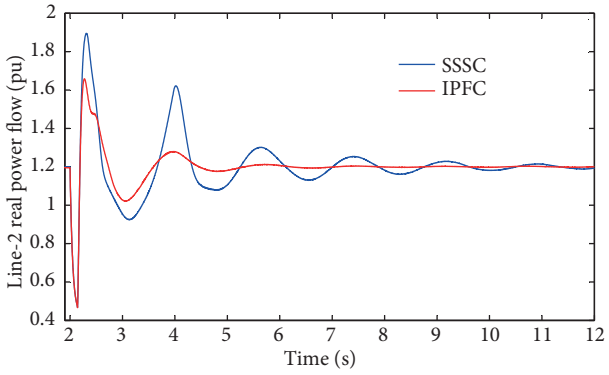

(c) Variation of Line-2 real power flow following three-phase fault

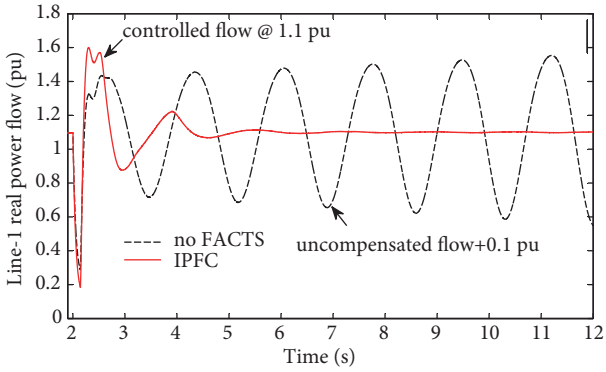

(d) Variation of Line-1 real power flow following three-phase fault

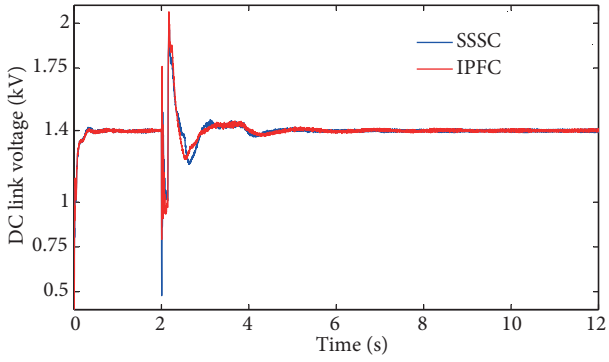

(e) DC link voltage excursions of two FACTS devices following three-phase fault

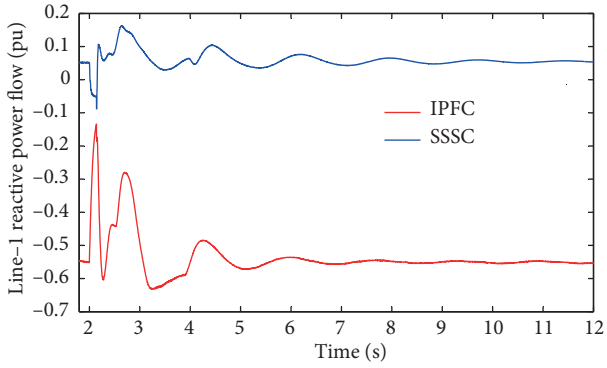

(f) Variation of Line-1 reactive power flow following three-phase fault

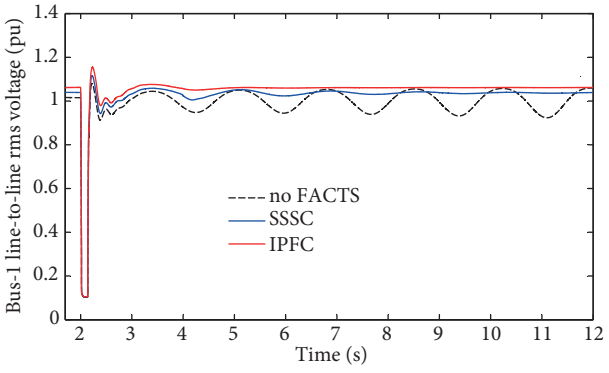

(g) Variation of Bus 1 voltage following three-phase fault

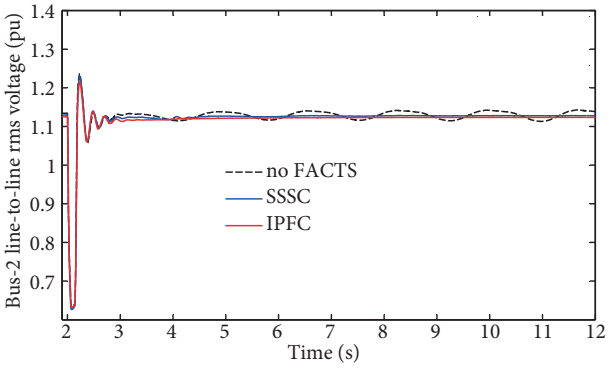

(h) Variation of Bus 2 voltage following three-phase fault

Figure 9. Simulated STFDC performance following three-phase fault.

show that STFDC-equipped IPFC better improves bus voltage profiles of the intertie with smoother responses following two-phase fault when compared with the STFDC-equipped SSSC.

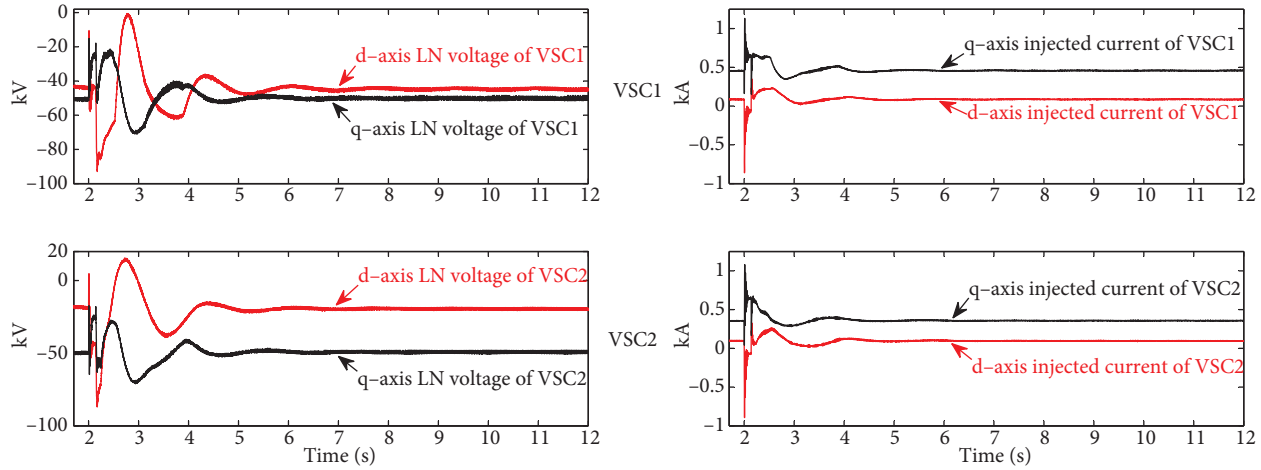

Figure 10. Simulated voltage and current waveforms of IPFC.

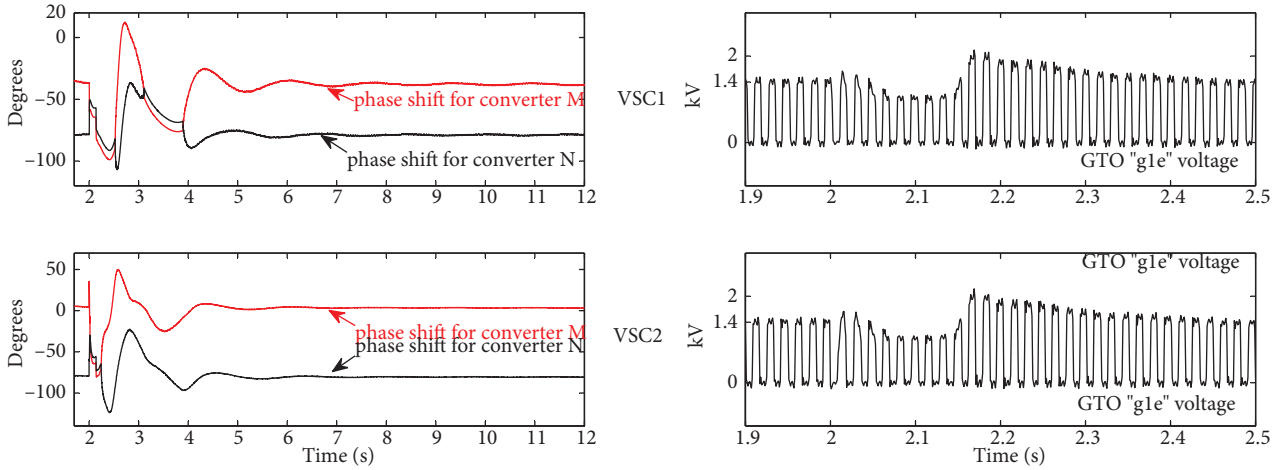

Figure 11. Simulated phase shift angles (ϕM and ϕN) and selected GTO's anode-to-cathode voltages of IPFC following three-phase fault.

5.3. Case 3: Single-phase to ground fault

The system is disturbed by a single-phase (phase C) to ground fault near Bus 1 on *Line-1* for 200 ms duration at $t = 2.0$ s, while keeping the same predisturbance steady-state operating conditions as in Case 1. This relatively longer fault makes the multimachine system operation unstable as large cumulative oscillations are observed both in time responses of generators' relative angles and real power flows of the intertie without any compensation scheme. In detail, Figures 13a and 13b show that the IPFC with STFDC robustly stabilizes the interarea mode of oscillations while the SSSC with STFDC shows a poor suppressing function. Figures 13c and 13d show that the IPFC endowed with the proposed STFDC eliminates the oscillations of the real power transmission of *Line-2* between the two areas and resumes the real power transmission to its controlled level before the fault. Figure 13e indicates that the DC link voltage controllers of both the SSSC and IPFC give

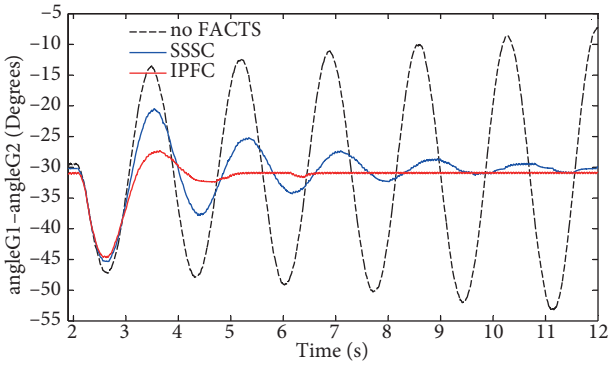

(a) Transient response of generator G2 rotor angle, measured with respect to generator G1 rotor angle following two-phase fault

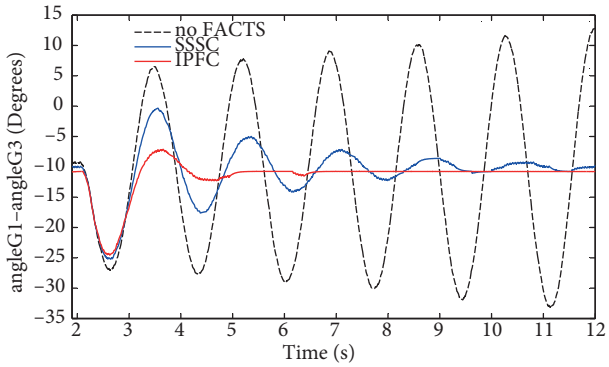

(b) Transient response of generator G3 rotor angle, measured with respect to generator G1 rotor angle following two-phase fault

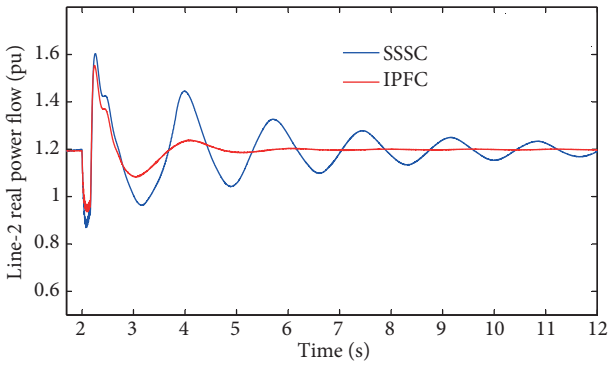

(c) Variation of Line-2 real power flow following two-phase fault

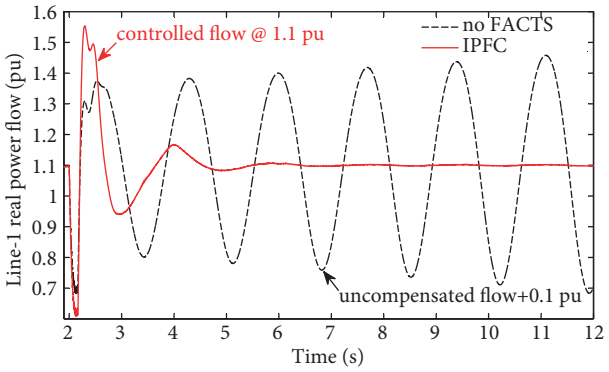

(d) Variation of Line-1 real power flow following two-phase fault

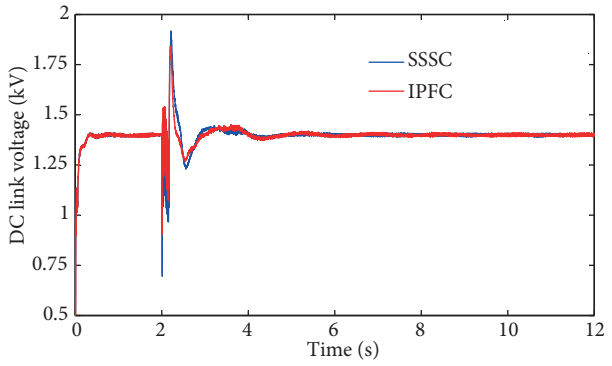

(e) DC link voltage excursions of two FACTS devices following two-phase fault

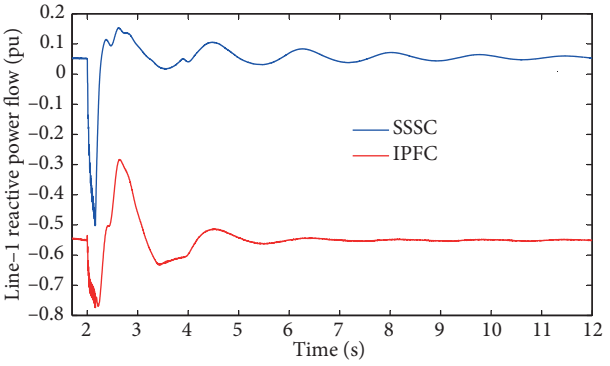

(f) Variation of Line-1 reactive power flow following two-phase fault

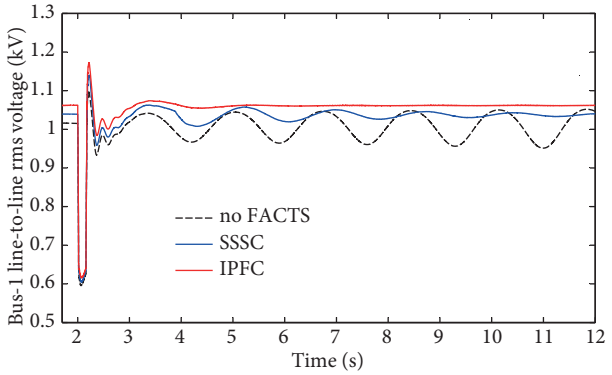

(g) Variation of Bus 1 voltage following two-phase fault

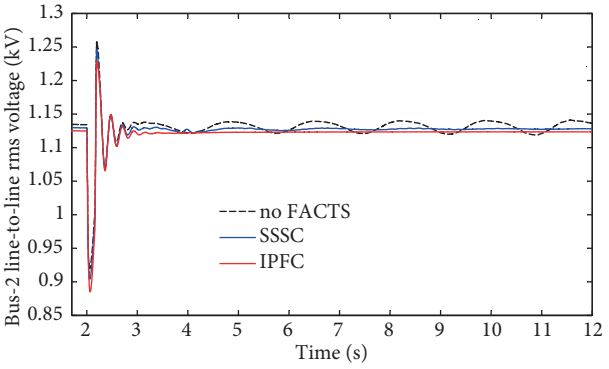

(h) Variation of Bus 2 voltage following two-phase fault

Figure 12. Simulated STFDC performance against two-phase fault.

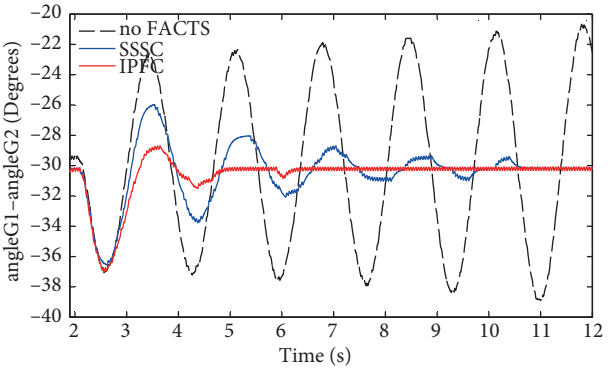

(a) Transient response of generator G2 rotor angle, measured with respect to generator G1 rotor angle following two-phase fault

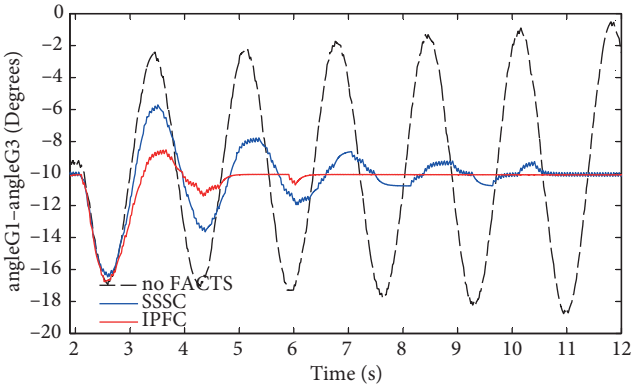

(b) Transient response of generator G3 rotor angle, measured with respect to generator G1 rotor angle following two-phase fault

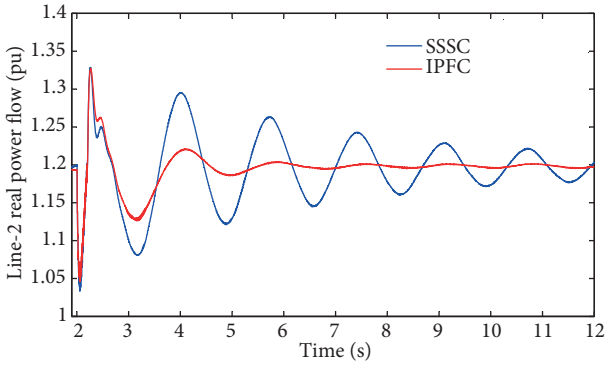

(c) Variation of Line-2 real power flow following two-phase fault

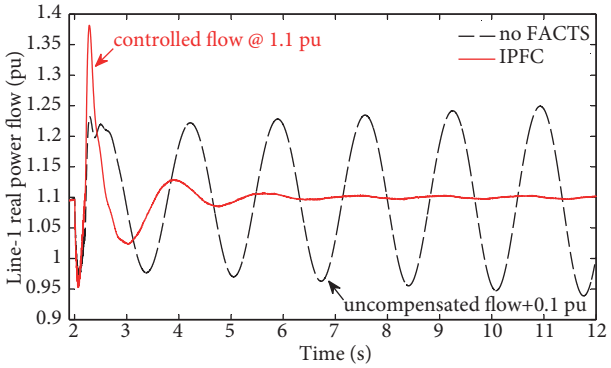

(d) Variation of Line-1 real power flow following two-phase fault

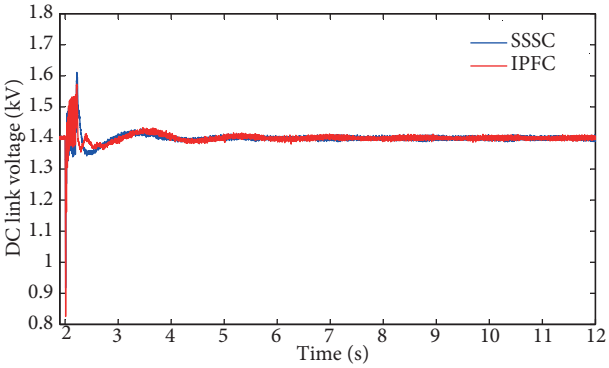

(e) DC link voltage excursions of two FACTS devices following two-phase fault

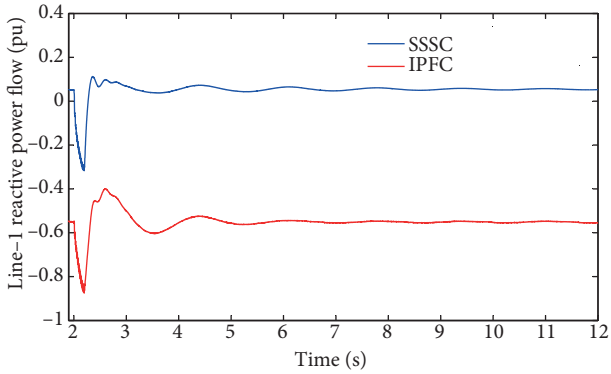

(f) Variation of Line-1 reactive power flow following two-phase fault

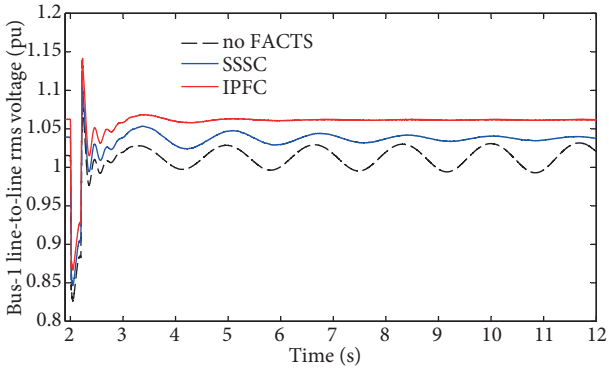

(g) Variation of Bus-1 reactive power flow following two-phase fault

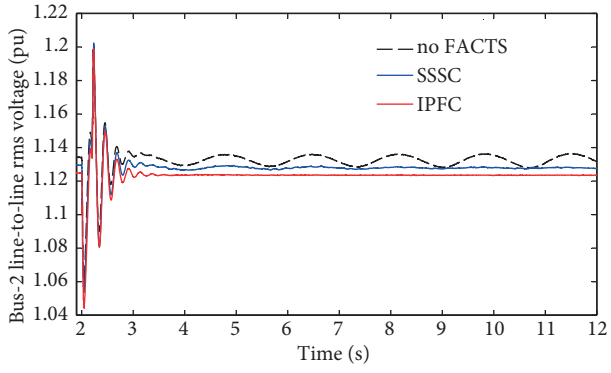

(h) Variation of Bus 2 voltage following two-phase fault

Figure 13. Simulated STFDC performance against two-phase fault.

practically the same response to the short circuit as in previous fault cases. Figure 13f shows reactive power flow fluctuations on *Line-1* when the IPFC and SSSC are operated separately when reactive power flow control function of the IPFC is disabled as in previous fault scenarios. It is shown that the reactive power fluctuations are practically the same for the two FACTS devices. Figures 13g and 13h show that the STFDC-equipped IPFC better improves bus voltage profiles of the intertie with smoother responses following single-phase fault when compared with the STFDC-equipped SSSC.

5.4. Total harmonic distortion (THD) content

Table 2 summarizes voltage distortions of *Buses 1* and *2* as a measure of THD. Records of the simulated cases taken at 12.5 s show that the THD values are within acceptable limits when the STFDC is activated in both control loops of the IPFC and SSSC [25]. Consequently, filtering is not required for the two FACTS devices even when GTOs are switched at the fundamental system frequency of 60 Hz.

Table 2. THD values of power system bus voltages.

Case 1	IPFC	THD for $V_{1(L-L)}$	THD for $V_{2(L-L)}$	SSSC	THD for $V_{1(L-L)}$	THD for $V_{2(L-L)}$
		0.29%	0.18%		0.20%	0.12%
Case 2		THD for $V_{1(L-L)}$	THD for $V_{2(L-L)}$		THD for $V_{1(L-L)}$	THD for $V_{2(L-L)}$
		0.25%	0.15%		0.20%	0.12%
Case 3		THD for $V_{1(L-L)}$	THD for $V_{2(L-L)}$		THD for $V_{1(L-L)}$	THD for $V_{2(L-L)}$
		0.12%	0.10%		0.12%	0.08%

6. Conclusion

The multiline power flow control function of the IPFC is enhanced with the simplex optimized STFDC to mitigate the interarea mode of oscillations in a multimachine power system. The performance of the damping scheme is verified using time-domain instantaneous responses of the system to various faults. It is demonstrated that the STFDC exhibits acceptable dynamic performance and improves overall system stability. Moreover, it is shown that the STFDC is robust to change in fault type and fault duration. The STFDC is further verified on the real power flow control loop of the SSSC, which also yields a particular performance comparison between the IPFC and SSSC. Although there is no voltage control function included in either the IPFC or SSSC operations, both are able to make voltages of the intertie buses less oscillatory in the case of severe faults. Successful operations of the IPFC and SSSC are proven by maintaining constant DC link voltage under fault scenarios. The quasi multipulse VSC designed for the FACTS devices does not disturb power quality in terms of harmonic content, which complies with the regulations. Hence, no filter is required at the line side.

References

[1] Kundur P. Power System Stability and Control. New York, NY, USA: McGraw-Hill, 1994.

[2] Mojtaba A, Morteza T. Full-adaptive THEN-part equipped fuzzy wavelet neural controller design of FACTS devices to suppress inter-area oscillations. Neurocomputing 2013; 118: 157–170.

[3] Shakarami MR, Kazemi A. Assessment of effect of SSSC stabilizer in different control channels on damping inter-area oscillations. Energy Convers Manage 2011; 52: 1622–1629.

[4] Lei X, Lerch EN, Povh D. Optimization and coordination of damping controls for improving system dynamic performance. IEEE T Power Syst 2001; 16: 473–480.

[5] Gyugyi L, Sen KK, Schauder CD. The interline power flow controller concept: a new approach to power flow management in transmission systems. IEEE T Power Deliver 1999; 14: 1115–1123.

[6] Jiang X, Fang X, Chow JH, Edris A, Uzunovic E, Parisi M, Hopkins L. A novel approach for modeling voltage-sourced converter-based FACTS controllers. IEEE T Power Deliver 2008; 23: 2591–2598.

[7] Murugan A, Thamizmani S. A new approach for voltage control of IPFC and UPFC for power flow management. In: IEEE 2013 International Conference on Energy Efficient Technologies for Sustainability; 10–12 April 2013; Nagercoil, India. New York, NY, USA: IEEE. pp. 1376–1381.

[8] Vural AM, Bayındır KÇ. A hybrid fuzzy-PI control scheme for a quasi multi-pulse interline power flow controller including PQ decoupling feature. J Power Electron 2012; 12: 787–799.

[9] Gyugyi L, Schauder CD, Sen KK. Static synchronous series compensator: a solid-state approach to the series compensation of transmission lines. IEEE T Power Deliver 1997; 12: 406–417.

[10] Jyothsna TR, Vaisakh K. Design and performance evaluation of SSSC supplementary modulation controller in power systems using SPEF method. Int J Electr Power Energy Syst 2012; 35: 158–170.

[11] Wang L, Truong DN. Comparative stability enhancement of PMSG-based offshore wind farm fed to an SG-based power system using an SSSC and an SVeC. IEEE T Power Syst 2013; 28: 336–1344.

[12] Kazemi A, Karimi E. The effect of interline power flow controller (IPFC) on damping inter-area oscillations in the interconnected power systems. In: IEEE 2006 International Symposium on Industrial Electronics; 9–13 July 2006; Montreal, Canada. New York, NY, USA: IEEE. pp. 1911–1915.

[13] Parimi AM, Elamvazuth I, Saad N. Interline power flow controller (IPFC) based damping controllers for damping low frequency oscillations in a power system. In: IEEE 2008 International Conference on Sustainable Energy Technologies; 24–27 November 2008; Singapore. New York, NY, USA: IEEE. pp. 334–339.

[14] Banaei MR, Kami A. Interline power flow controller based damping controllers for damping low frequency oscillations. In: IEEE 2009 31st International Telecommunications Energy Conference; 18–22 October 2009; Incheon, South Korea. New York, NY, USA: IEEE. pp. 1–6.

[15] Veeramalla J, Sreerama-Kumar R. Application of interline power flow controller (IPFC) for damping low frequency oscillations in power systems. In: IEEE 2010 International Symposium on Modern Electric Power Systems; 20–22 September 2010; Wrocław, Poland. New York, NY, USA: IEEE. pp. 1–6.

[16] Parimi AM, Elamvazuthi I, Saad N. Fuzzy logic control for IPFC for damping low frequency oscillations. In: IEEE 2010 International Conference on Intelligent and Advanced Systems; 15–17 June 2010; Kuala Lumpur, Malaysia. New York, NY, USA: IEEE. pp. 1–5.

[17] Belwanshi SM, Chandrakar VK, Dhurvey SN. Performance evaluation of IPFC by using fuzzy logic based controller for damping of power system oscillations. In: IEEE 2011 4th International Conference on Emerging Trends in Engineering and Technology; 18–20 November 2011; Port Louis, Mauritius. New York, NY, USA: IEEE. pp. 168–173.

[18] Parimi AM, Sahoo NC, Elamvazuth I, Saad N. Dynamic modeling of interline power flow controller for small signal stability. In: IEEE 2010 International Conference on Power and Energy; 29 November–1 December 2010; Kuala Lumpur, Malaysia. New York, NY, USA: IEEE. pp. 583–588.

[19] Parimi AM, Sahoo NC, Elamvazuth I, Saad N. Transient stability enhancement and power flow control in a multi-machine power system using interline power flow controller. In: IEEE 2011 International Conference on Energy, Automation, and Signal; 28–30 December 2011; Bhubaneswar, India. New York, NY, USA: IEEE. pp. 1–6.

[20] Shan J, Gole AM, Annakkage UD, Jacobson DA. Damping performance analysis of IPFC and UPFC controllers using validated small-signal models. IEEE T Power Deliver 2011; 26: 446–454.

[21] Vural AM, Bayındır KÇ. Two-level quasi multi-pulse voltage source converter based generalized unified power flow controller. Int Rev Electr Eng 2011; 6: 2622–2637.

[22] Hagiwara M, Fujita H, Akagi H. Performance of a self-commutated BTB HVDC link system under a single-line-to-ground fault condition. IEEE T Power Electr 2003; 18: 278–285.

[23] Mudi RK, Pal NR. A robust self-tuning scheme for PI- and PD-type fuzzy controllers. IEEE T Fuzzy Syst 1999; 7: 2–16.

[24] Hameed S, Das B, Pant V. A self-tuning fuzzy PI controller for TCSC to improve power system stability. Electr Pow Syst Res 2008; 78: 1726–1735.

[25] IEEE. Recommended Practices and Requirements for Harmonic Control in Electrical Power Systems. New York, NY, USA: Institute of Electrical and Electronics Engineering, 1993.